IEEE Access
Multidisciplinary ⋮ Rapid Review ⋮ Open Access Journal

Received February 24, 2022, accepted May 8, 2022, date of publication May 16, 2022, date of current version May 23, 2022.

*Digital Object Identifier 10.1109/ACCESS.2022.3175210*

# Distributed Force Measurement and Mapping Using Pressure-Sensitive Film and Image Processing for Active and Passive Aligners on Orthodontic Attachments

**N. SYAHIRA M. ZAMANI[1], ASMA ASHARI[2], SAWAL HAMID MD ALI[1], (Member, IEEE), KOK BENG GAN[1], (Member, IEEE), REUBEN AXEL WEE MING HOW[3], ROHAYA MEGAT ABDUL WAHAB[2], ALIZAE MARNY FADZLIN SYED MOHAMED[2], SINDHU SINNASAMY[4], AND MOHD HADRI HAFIZ MOKHTAR[1], (Member, IEEE)**

[1]Department of Electrical, Electronic and Systems Engineering, Faculty of Engineering and Built Environment, Universiti Kebangsaan Malaysia, Bangi 43600, Selangor, Malaysia
[2]Department of Family Oral Health, Faculty of Dentistry, Universiti Kebangsaan Malaysia, Kuala Lumpur 50300, Malaysia
[3]WhiteSmileclear Laboratory Services, Berjaya Times Square, Kuala Lumpur 55100, Malaysia
[4]Faculty of Dentistry, Mahsa University, Bandar Saujana Putra, Jenjarom, Selangor 42610, Malaysia

Corresponding authors: Mohd Hadri Hafiz Mokhtar (hadri@ukm.edu.my) and Asma Ashari (asmaashari@ukm.edu.my)

This work was supported in part by the National Industrial Fund under Grant DD-2019-012, and in part by Universiti Kebangsaan Malaysia (UKM) Matching Collaboration Fund under Grant DPK-2020-003.
This work involved human subjects or animals in its research. Approval of all ethical and experimental procedures and protocols was granted by the Research Ethics Committee, The National University of Malaysia, under Application No. UKM PPI/111/8/JEP-2021-410, and performed in line with the International Conference of Harmonization Good Clinical Practice Guidelines.

**ABSTRACT** Orthodontic clear aligners, along with their attachments, are used for the corrective alignment of teeth during orthodontic treatment. Although the clear aligner technique has gained widespread popularity due to its aesthetic quality, studies that examine and map the measurement of forces applied to clear aligner attachments are lacking. This investigation describes the topographical visualisation of the force in clear aligner attachments. We describe a method using Prescale® pressure film and an image processing technique to obtain the topographical visualisation of a clear aligner's distributed force on the attachment in an in-vitro study using resin models. The variation of colour density due to the distributed force is calibrated with a force gauge for validation. The image processing technique is demonstrated through the histogram-based K-means clustering method with 3D visualisation of the distributed force. This method involves pressure film calibration, followed by sample preparation and image processing analysis. The proposed topographical pressure mapping system illustrates the distributed force on the clear aligner attachment as the force applied is directly proportional to intensit. For active aligners, the mean force ranged from 6.2–6.3 N, and for passive aligners, the mean force ranged from 4.8–4.9 N. Therefore, the net force exerted on a single clear aligner attachment in a resin model for this study was 1.3–1.4 N. The preliminary findings of this work can be developed further to be a reference in future clinical orthodontic clear aligner and attachment research.

**INDEX TERMS** Image colour analysis, image processing, orthodontic clear aligner, force measurement.

## I. INTRODUCTION

Clear orthodontic aligners and their attachments are used to adjust tooth alignment during orthodontic treatment. Malocclusion is defined as the misalignment of the teeth of the upper and lower dental arches. Orthodontics aims to correct malocclusions using orthodontic appliances are used. Clear aligners, alternatives to fixed appliances to treat malocclusions, are gaining widespread popularity. Patients have indicated their preference for clear aligners over conventional

The associate editor coordinating the review of this manuscript and approving it for publication was Abdullah Iliyasu.

fixed appliances is due to aesthetics [1], [2]. Less pain was also reported [3]. Furthermore, clear aligners are the chosen therapy for adults at risk for periodontitis and gingivitis [4]. Additionally, clear aligners rarely cause emergencies, yielding less chairside time, which is a great advantage for clinicians [3]. In the next sub-sections, we discuss on the clear aligners, method force measurement using image processing method or electronic methods.

### A. CLEAR ALIGNERS

Clear aligner therapy has been shown to be more challenging than fixed appliances to address extrusive movements, rotations of rounded teeth and the buccolingual inclination of anterior teeth [3], [5], [6]. In addition, limitations exist with clear aligners when treating intrusion and severe overbites [7]. The systematic review by Rossini *et al.* also included studies of attachments to increase the accuracy and predictability of tooth derotations in clear aligner therapy. The forces and pressures exerted upon a tooth have been widely researched to understand the levels required for orthodontic tooth movement. The toot's supporting structures, such as the alveolar bone and periodontal ligaments, are subjected to these forces as well [5], [8]. Hence, the exerted forces and pressures should be within normal limits to minimise any iatrogenic damage to the teeth. Therefore, measurements of the distributed forces exerted by the clear aligners onto the attachments on the teeth are useful, and the toot's movements, such as rotational and de-rotational shifts, can be better understood. This procedure achieves the desired tooth movement per the corrective protocol prescribed by the orthodontist, yielding minimal damage to the teeth.

### B. FORCE MEASUREMENT IN ORTHODONTICS USING PRESCALE FILM

The Fujifilm Prescale® products have been widely used in occlusion, bite force recording, temporomandibular joints, and orthodontic [9]–[12]. Jalalpour *et al.* [13] concluded that thecontact pressure could be measured by the thermal contact resistance, whereby a high torque produces a dark stain concentration.

Barbagallo *et al.* proposed a similar pressure film approach to measure the force on removable thermoplastic appliances (RTA) [14] using Pressurex® film. They studied patients with palatally displaced first premolars treated with a series of four active appliances for eight weeks. The forces exerted by a clear aligner onto the first premola's palatal surface were quantified using digital imaging and spectrophotometry analyses. The image stains of the pressure sample were taken using AnalySIS Soft Image System software, employing spectrophotometry to calculate the colour intensity threshold. A calibration curve showed that the known pressure applied was directly proportional to concentration based on the spectrophotometry analysis. However, the findings were limited to force measurement observations as no topographical mapping of force was provided.

A recent study by Cervinara *et al.* [12] used Fujifilm Prescale® on an upper right incisor, using three-dimensional (3D) printed resin casts to identify and quantify high-pressure areas from a clear aligner. However, the models required that a thin layer was removed to accommodate the film, likely affecting the accuracy of the results. This study applied Fujifilm FPD-8010E analysis software. The analysis system scans the prescale film, digitising and storing the scanned results of the images [12]. The output of the analysis was presented as a flat two-dimensional (2D) image of pressure mapping that visualised the teet's appearance with colour levels of stain. This method was also limited to determining the pressure level without 3D visualised mapping.

### C. IMAGE PROCESSING OF PRESCALE FILM

An important aspect of prescale film analysis is the image processing technique used to scan and identify the film's colour brightness. Image processing through computer vision has been widely implemented in various applications, especially in the medical imaging field. The image segmentation technique is used for the detection of abnormal tissue, such as from a brain tumour, with magnetic resonance imaging (MRI) [15]–[17] and for the identification of leukaemia cells [18].

Image segmentation is crucial in image processing to extract and analyse the region of interest (ROI). This technique can be performed on a grayscale image through monochrome image segmentation or colour image through colour image segmentation [19], [20]. Real-time application of monochrome image segmentation has been proposed using the watershed algorithm. [21]. However, colour image segmentation provides more information on the intensity of a pixel than a grayscale image represented by a histogram [22], [23].

Generally, colour image segmentation involves three primary colours in the 'colour space', namely red, green and blue (RGB). There are several well-known colour spaces besides RGB, namely HSV and Lab [24]. HSV colour space represents the hue, saturation, and value of the image. In the Lab colour space,'L' indicates luminance or brightness,'a' indicates the amount of green or red, and 'b' indicates the amount of blue or yellow in the image [23], [25], [26].

Colour image segmentation can be used as a measurement tool through clustering, spatial clustering and schemes of split-and-merge [27]. Clustering is an unsupervised learning method in machine learning, widely studied in computer vision [28]–[30]. In this approach, the image features are learned from unlabelled data [31], [32]. The most commonly used clustering method is the K-means clustering method [15], [20], [33], [34], which is a clustering algorithm developed in the 1950s and named by James MacQueen in 1967 [35]. Research on'K-mean' clustering method was reviewed by Yuan and Yang in 2019 to select the k-value method [36]. This algorithm finds the image features by grouping the image pixels and locating various features from an existing object, form or colour in the image.

### D. ELECTRONIC FORCE SENSORS

Apart from using prescale films, other methods have been proposed to measure forces in orthodontic treatment, such as the use of flexi-force electronic sensors [12], [37]–[39]. Although some authors have demonstrated the attempt to quantify the force [37], [40]–[42], the visualisation of the mechanical force is a challenge due to the small form factor of the attachment. Extensive studies have been conducted to simulate the moment and torque using the finite element technique and numerical methods [12], [43]–[46]. The attachments also proved beneficial when intraoral elastics were used, optimising aligner fit and minimising uncontrolled intrusion [47]. Uniform compression areas along the root surfaces were also observed with the presence of composite attachments [48].

In another study that measured forces in orthodontic treatment, a modular force-torque device was developed, which was used in several follow-up studies [49]–[51]. This device was complemented by a goniometer that helped simulate the tipping sequence. In addition, a sensor measuring the force components was fixed in the device. A three-point bending recovery system was also used to measure the clear aligner material's resilience quantified as force and energy generated [52]. This method was preceded by a study that used a small force sensor embedded on the studied tooth to measure forces [53], which affected the properties of the contact surfaces.

From the literature, the use of electronic sensors to measure the localised force is possible. However, an electronic sensor will only provide a localised force measurement that requires electronic signal conditioning. Therefore, this method is not practical for orthodontic applications since clear aligners apply pressure in several areas to allow tooth movement. In addition, this method cannot determine the distributed force mapping because of the form factor of the sensitive area.

Based on the review of these methods, we propose the use of prescale film to obtain an accurate distributed force measurement in an orthodontic resin model. The proposed method integrates the following technical contributions. First, this method can produce a contour-based topographical force mapping that is useful for force evaluation by orthodontists. Second, based on the image processing technique, we can determine the exact force value at a critical point on the aligner to predict the rotational or lateral movement of the tooth. Third, other aligner companies have conducted predictive topographical mapping to visualise the forces, showing how the aligners and their attachments operate. Having a more accurate method would prove technically and commercially beneficial. Fourth, this method will be a beneficial tool in exploring research involving clear aligners via topographical mapping. This study aims to perform a topographical force mapping and determine the range of forces involved in the two attachment types in clear aligners in the lab setting. This study proposes the K-means clustering algorithm in combination with applying the prescale film from Fujifilm to visualise the force mapping exerted by the aligner onto the attachments.

## II. METHODOLOGY

This study was approved by the Research Ethics Committee of the Universiti Kebangsaan Malaysia (UKM) (Reference Number JEP-2021-410). We obtained the clear aligners and resin models from the WhiteSmile Clear LaboratoryServices, Visivest Sdn Bhd (07-51 Berjaya Times Square, 1 Jalan Imbi, 55100 Kuala Lumpur Malaysia). The aligners were made of Tristar material which is the latest generation of multilaminate materials. It is formulated by combining different layers of thermoplastic polyurethanes, thermoplastic elastomers, and polyethylene terephthalate glycol (PETG). This combination achieves a high elastic limit, low'creep and flow', and low force decay throughout the application.

The resin model was created using a scan of an anonymous patient. Most of the teeth in the resin model were removed before applying the aligners to record the pressure specific to the attachments. This procedure minimises interferences in clear aligner therapy, where complex interactions can occur between other teeth and aligners. By reducing interferences, the pressures exerted over a single tooth can be better quantified.

In this study, passive and active clear aligners were tested. Passive aligners are not used in the real clinical scenario since they do not have any sculpting on the attachments that will produce an additional force from the aligner. The passive aligner was chosen such that initial passive forces upon seating of the aligner can be measured against an active aligner with active orthodontic attachments. The difference of forces yields the absolute force from the aligner attachments. Three passive aligners of rectangular and ellipsoidal attachments for both active and passive were used to measure the forces. The sculpting of the resin models to produce the active aligners is shown in Fig. 1.

During the thermo-press process, the sculpted area of the resin model with 30 $\mu$m in-depth causes the active aligner to be suctioned into the dimpled area. This process creates an increased thickness, therefore producing an additional force from the aligner to rotate the tooth in question. When the active aligner is placed onto the original non-sculpted attachment on the resin model, it will apply a localised force onto the attachment. For this study, we only focused on the sculpted area of the attachment, which is the area of interest.

Fujifilm pressure-sensitive film was utilised in this experiment, composed of two film types: A-film and C-film. A-film is a coated base of colour-forming material that consists of microcapsules, while the C-film is a coated base of colour-developing material [38], [54]. The coated sides of the two films need to be placed facing each other before the force is applied to generate a pink stain. A pink stain forms when the microcapsules burst from the reaction between the colour-forming and the colour-developing materials [55]. In this study, the A- and C-films were attached and inserted between the clear aligner and the 3D resin teeth model. As the pressure

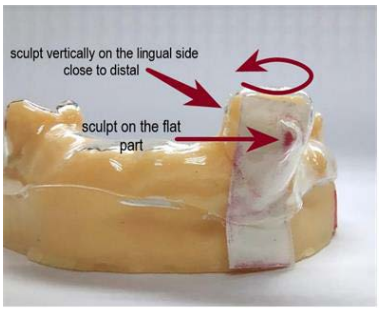


(a) Ellipsoidal attachment

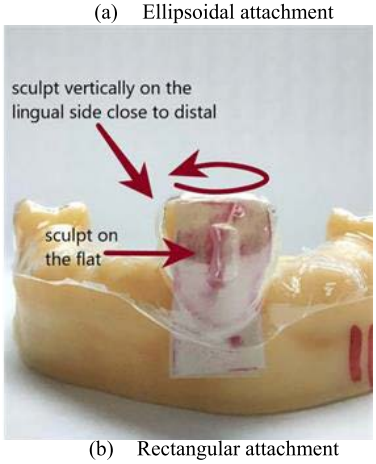


(b) Rectangular attachment

**FIGURE 1.** Sculpted area of an active aligner that will move the tooth of a) ellipsoidal attachment and b) rectangular attachment.

film was inserted, a stain developed from pressure in the area. Therefore, the pressure presented by the stain was measured by the calibration method described in the following section.

### A. CALIBRATION OF PRESCALE FILM AND FORCE MEASUREMENT

The experimental design involved the apparatus preparation, thedetermination of force magnitude, force implementation, and the analysis of pressure film using the image processing approach. In addition, the intra-correlation coefficient (ICC) was used to assess intra- and inter-rater reliability.

#### 1) FORCE GAUGE CALIBRATION KIT

Fig. 2 shows the setup of the steel stand with a force gauge (Sauter FH 10UK Force Gauge) attached. The force gauge has a resolution of 0.005 N and a maximum force of 10 N. The wheel located at the top of the stand controls the force gauge height. When the wheel is rotated, the force gauge moves down or up. This movement then applies a specific force value onto the pressure film. The embedded electronic sensor measures the applied force at the end of the force gauge. With this method, the force applied to the active and passive attachment for ellipsoidal and rectangular aligners could be measured. The calibration curve has a linear relationship between the number of red pixels and the pressure applied, meaning a higher applied pressure causes more bubbles to burst. Hence, the pixel value increases.


**FIGURE 2.** Steel stand and force gauge for force calibration kit.

#### 2) THE MAGNITUDE OF FORCE MEASUREMENT

This experiment was conducted using a 'super low pressure' film type indicated by the LLW code. The 'L' indicates low pressure, and the 'W' indicates the presence two film sheets. The LLW pressure film is sensitive, whereby the maximum force that can be applied is 10 N. A total of five force readings were selected for this experimental setup. For the calibration, the magnitudes of force applied to the film were 2.125, 4.325, 6.114, 8.080 and 9.600 N, as measured by the force gauge. The purpose of this calibration is to establish a relationship between the calibrated forces and the resultant stains on pressure film. This procedure is needed for the baseline measurement of the force exerted by the clear aligner and the ellipsoidal attachment for the active and passive cases.

### B. IMAGE PROCESSING APPROACH

This sub-section explains the proposed setup to perform force mapping by analysing the sample image through an image processing approach, including pre-processing, clustering, colour segmentation, the elimination of illumination, colour space conversion for ROI intensity and 3D topographical mapping, as depicted in Fig. 3.

#### 1) DATA SAMPLE ACQUISITIO

Fig. 3 shows the setup for the image acquisition technique used to analyse the prescale film. An image sample of the resin model of the tooth with the placement of the clear aligner was captured using a high-resolution Sony micro-lens DSC-QX10 camera. The resin model and the camera were placed in a mini studio box with a controlled brightness from the LED array. The camera was wirelessly connected to an Android smartphone via a near field communication (NFC) connection. The three points of view for image acquisition

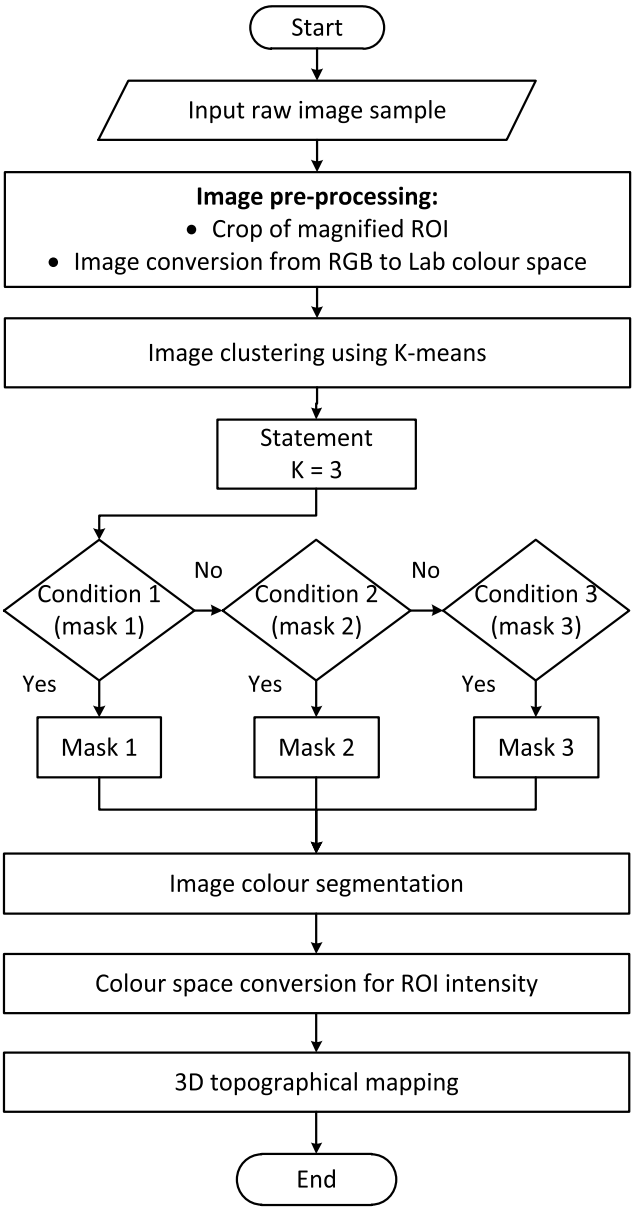


**FIGURE 3.** Block diagram of image processing approach.

setup are the plan, front and side views. In addition, the force indicator's image was captured from the same views as the image sample of the clear aligner attachment. The micro-lens Sony camera setting was controlled with a smartphone using the Imaging Edge Mobile app. In addition, the white-balance and auto-focus settings were engaged when capturing the image.

### 2) PRE-PROCESSING IMAGE PROCESS

The pre-processingimage process requires cropping the image sample according to the ROI, where the red-stained region is desired to remove the unwanted background so that the algorithm would focus on the foreground. As a result, a cropped image typically has some loss in image resolution. However, the'Initial Magnificatio' parameter was adopted to

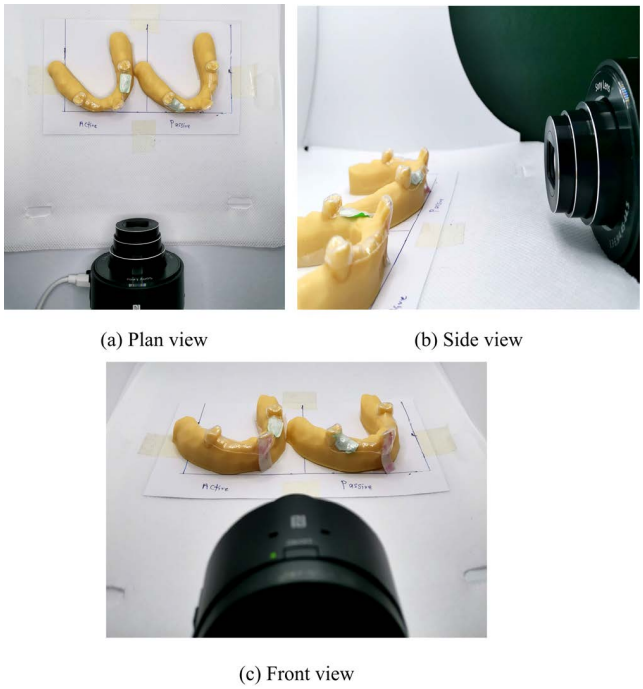

(a) Plan view (b) Side view

(c) Front view

**FIGURE 4.** Image sample acquisition.

maintain the image resolution, as the image was magnified to a specific region from the input image.

The cropped ROI image of the pinkish stain is in RGB colour space. Various colour space conversions can identify and visualise specific colours, such as RGB, HSV and Lab, as illustrated in Fig 5. In our case, Lab colour space was more appropriate for the colour space conversion to perform the clustering method.

### 3) K-MEANS IMAGE CLUSTERING AND SEGMENTATION

The Lab colour space is a three-axis colour system that contains dimensions 'L' that indicates lightness, while 'a' and 'b' indicate colour dimensions. All colours in the spectrum are included within the 'a' and 'b' colour spaces. Using the K-means clustering method, this colour space filters the image with a clustered index based on different colour intensities. Each object has a location in space. The K-means clustering method finds and partitions such objects within each cluster as close as possible and as far as possible from objects in other clusters using the objective function *J,* as in (1).

$$J = \sum_{j=1}^{k} \sum_{i=1}^{n} \left\| x_i^{(j)} - c_j \right\|^2 \tag{1}$$

where k indicates the number of clusters, $n$ indicates the number of cases and the term $\left\| x_i^{(j)} - c_j \right\|$ represents distance function.

The ROI was selected using colour image segmentation through image RGB conversion to Lab colour space using the K-means clustering method, as illustrated in Fig. 3. Three initial 'K' values were used in the K-means clustering process. The clustering was performed to identify the objects

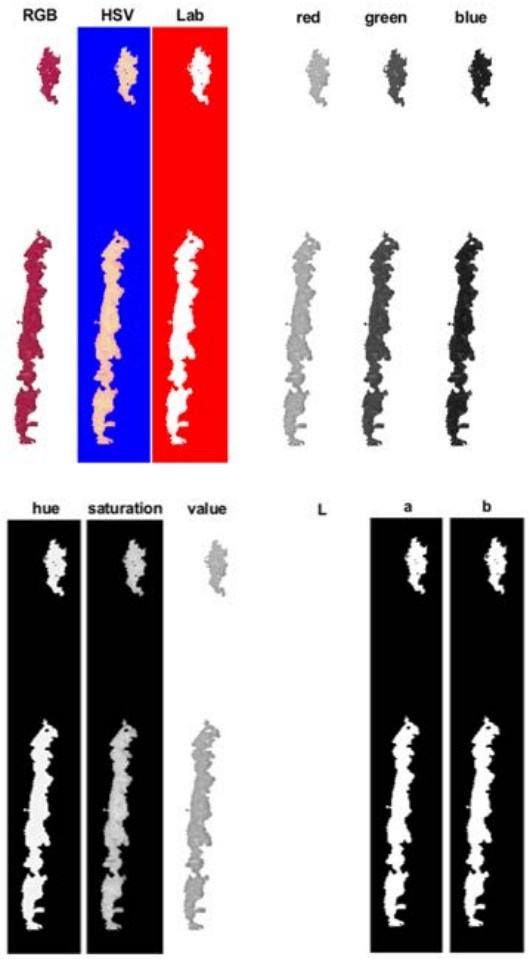


**FIGURE 5.** Image sample acquisition.

or regions inside the image sample. Given three conditions (three clusters), the user must identify and select the foreground mask (exact ROI). The selected mask was converted into a binary version to extract the image noise through the 'L' space since the ROI is in the Lab colour space. Nevertheless, no background subtraction with a specific method is involved in this conversion. A binary version rescales the image into black (0) and white (256) pixels by default using Otsu's threshold method using (2). Otsu's method chooses the threshold value by an intraclass variance of the black and white pixels [56].

$$g(x,y) = \begin{cases} 0, & \text{if } f(x,y) \quad < T \\ 1, & \text{if } f(x,y) \quad \geq T \end{cases} \tag{2}$$

where $x$ and $y$ represent a grey value, $T$ represents a threshold value, g($x$,$y$) is the threshold image, and $f$($x$,y) is the input image.

#### 4) COLOUR SPACE CONVERSION FOR ROI INTENSITY

Next, to index the intensity colour, the final output of the segmented mask was reverted into the original colour space, which is RGB, as indicated in Fig. 3. The segmented ROI image input data matrices were converted to an intensity image. However, to illustrate an image mapping, the image's colour in the RGB channel needed to be assigned to the HSV colour space conversion using (3). HSV was chosen because of the high clarity of pixel intensity in the saturation channel.

$$H = \begin{cases} \frac{\left(\frac{G'-B'}{\text{MAX}-\text{MIN}}\right)}{6}, & \text{if } R' \quad = \text{MAX} \\ \frac{\left(2+\frac{B'-R'}{\text{MAX}-\text{MIN}}\right)}{6}, & \text{if } G' \quad = \text{MAX} \\ \frac{\left(4+\frac{R'-G'}{\text{MAX}-\text{MIN}}\right)}{6}, & \text{if } B' \quad = \text{MAX} \end{cases} \tag{3}$$

$$S = \frac{\text{MAX} - \text{MIN}}{\text{MAX}}$$
$$V = \text{MAX}$$

The MAX and MIN indicate the $R'G'B'$ triplet, which are the conditional statements for maximum and minimum red, green, and blue values, respectively. The RGB values ranging from 0 to 255 are converted to HSV. Unlike the RGB, HSV values range in different perspectives. The 'Hue' component represents a variety of colours from 0 to 360 degrees. The 'Saturation' component illustrates the intensity of a colour ranging from 0 to 1. Lastly, the 'Value' component describes the brightness of a colour.

Here, the image intensity level could be visualised according to the colour range. Hence, a 2D topographical map of the intensity level could be created.

#### 5) INTENSITY TO FORCE MEASUREMEN

Based on the force calibration, the intensity level could then be converted into a force. The relationship was evaluated by the histogram and the calibration curve of the force versus red pixels. Red pixels are the colour of prescale, representing the force region. Hence, the outcome of the relationship would determine the proportions between intensity and force measurement.

#### 6) 3-D TOPOGRAPHICAL MAPPING

The distributed height of the image surface was visualised by implementing a MATLAB function called *mesh*. The *mesh* function creates a 3D surface plot, a grid figure in the $xy$–plane defined by the mesh of $X$ and $Y$. The $Z$-axis represents the imag's colour level (intensity) displayed by the surface height derived from the 'Saturation' channel of the HSV colour space. Based on the calibration of prescale measurements, the graph relationship between the pixel level and the force applied was generated from the intensity of the segmented image. Hence, the force could be determined from the indexed intensity colour level. Therefore, the force's magnitude is shown on the $Z$-axis of the 3D topographical based on the relationship between intensity level and force indicator reading obtained from the calibration curve.

In the 3D map, the image is assigned by sets (active and passive for both rectangular and ellipsoidal). A three-column matrix of RGB triplets specifies a custom colourmap where each row indicates one component colour – red, green and blue. From the saturation channel intensity, the indexed coloured ROI that ranges from 0 to 1 indicates the force in Newtons. Finally, the force is distributed based on a generalised extreme value (GEV). The GEV consists of three parameters – $k$ (shape), sigma ($\sigma$-scale) and ($\mu$-location). This distribution represents a measurement or observation to evaluate the mean value of the force absent using (4):

$$\mu = \frac{1}{N}\sum_{i=1}^{N} A_{i.} \tag{4}$$

where symbol represents the population mean, and the $N$ is the total number of exact values of the force. Meanwhile, the symbol $\sum$ indicates the sum of all population scores (force value), and $A$ represents a force value.

## III. RESULTS AND DISCUSSION

The intraclass correlation coefficient (ICC) for the intra- and inter-rater reliability for force measurements wasabove 0.95, which suggests very good reliability. In this experimental work, the proposed force measurement system was analysed using the image processing approaches. The following analysis focused on the calibration of the absolute force measurement on the sample of five applied forces. The same procedure was applied to the clear aligner and the 3D model teeth with active and passive attachment based on this force calibration measurement.

### A. FORCE INDICATOR BARS COLOUR CLUSTERING AND SEGMENTATION

Using the 'Initial Magnificatio' parameter, each force indicator reading in Fig. 6 was cropped according to the ROI. This figure was obtained during the calibration setup. This parameter prevents quality loss after cropping, as the cropped image was displayed by magnifying the initial image. Fig. 7(a) shows the cropped image of five force indicators taken with the same setting as the clear aligner photos. Here, each indicator is cropped separately for clarity. The cropped force indicators depict the increasing stain-coloured areas from low to high forces as measured based on the burst of the pressure film bubbles.

As we implement k-means using Lab colour space, three masks (conditions) were assigned in an image sample consisting of two backgrounds and one foreground, as illustrated in Fig. 6 (b). Fig 7 shows a sample of three clusters from the ROI method described previously, where the subjected ROI (foreground) is labelled in the white mask, cluster 3. By user input, the subjected ROI was selected.

Generally, the selected ROI was in the RGB colour space, which was converted into the HSV colour space. This conversation was chosen because of the advantage of the saturation channel in HSV colour space that can illustrate the radiation of colour intensity, as shown in Fig. 9. The saturation channel

**FIGURE 6.** Sample of a force indicator.

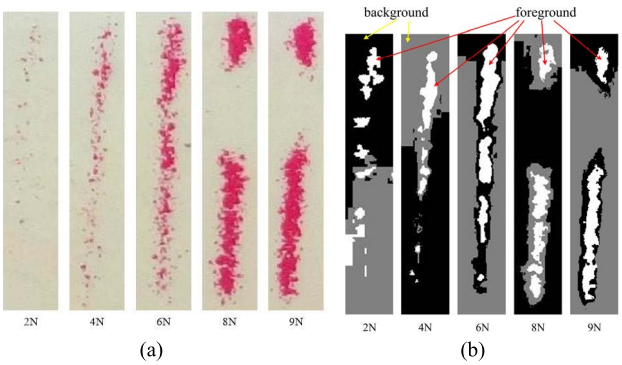


**FIGURE 7.** Cropped (a) and clustered index (b) of ROI image for five force indicators, 2, 4, 6, 8 and 9 N (from left to right).


**FIGURE 8.** A sample of a) cluster index, (b) cluster 1 represent background 1, (c) cluster 2 represent background 2, and (d) cluster 3 represent foreground.

produces a pure red, green or blue pixel [57], and the colour of this stain is mostly red. The colour intensities of high forces (8 to 9 N) have high brightness in almost all areas. Meanwhile, low forces of 2 to 6 N depict low brightness and only cover a relatively small exposure area. Based on the observation of each force indicator sample, we can conclude that high and low forces produce bright and dim colour intensities, respectively.

### B. 2D MAPPING OF FORCE INDICATOR

The indexing of colours was performed for each force indicator to visualise the level of colour intensity. The colour index

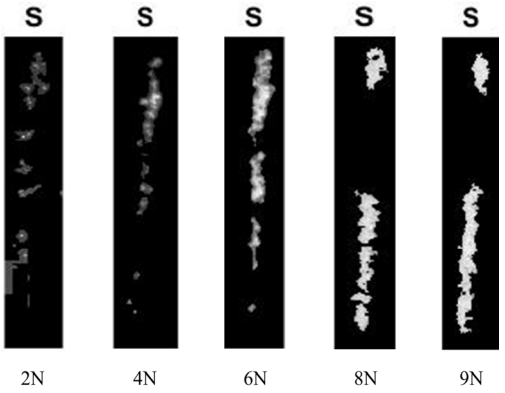


**FIGURE 9.** Radiation of colour intensity on saturation of HSV colour space for 2, 4, 6, 8, and 9 N (from left to right).

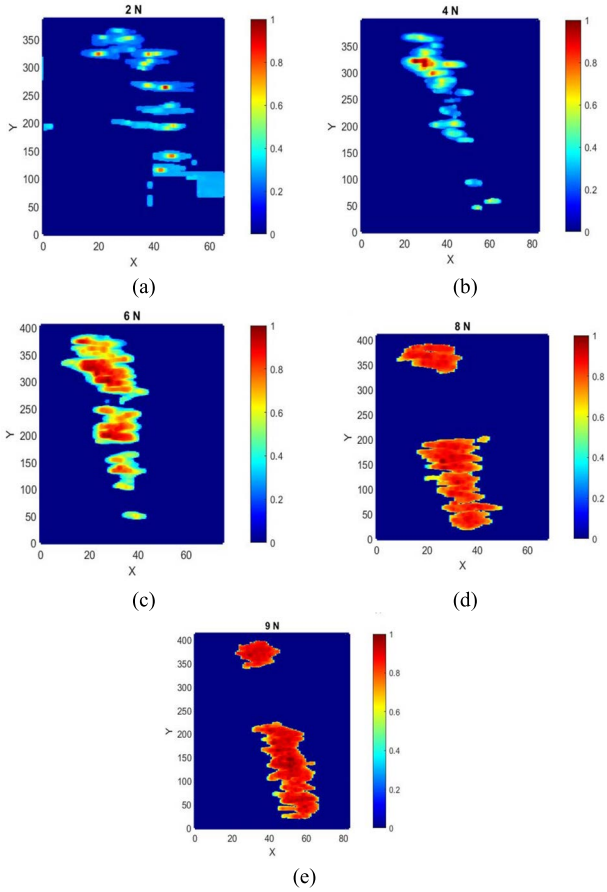


**FIGURE 10.** 2D topography map to show intensity levels.

is scaled from 0 to 1.0, as depicted in the 2D topographical map in Fig. 10. The high force is shown as having a larger, red-coloured area (Fig. 10(e)), which signifies a higher colour intensity compared to the low force (Fig. 10(a)). The colour intensity level shows a similar visual representation to the initial cluster index images but differs in brightness. This difference is due to the larger forces covering more areas with higher colour intensity, indicating high pressure. A range value of intensity level was scaled by a colour map array called the 'jet' code to differentiate the intensity levels.

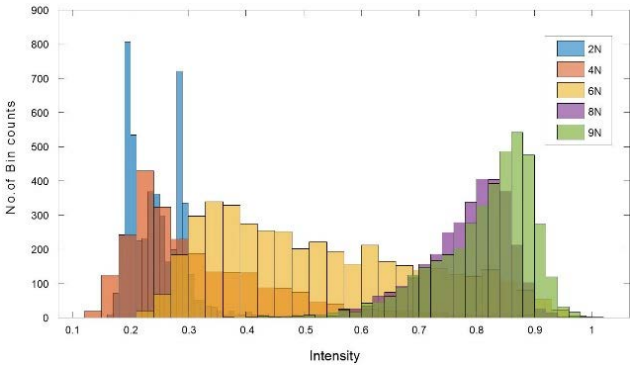


**FIGURE 11.** Histogram of the merge force indicator.

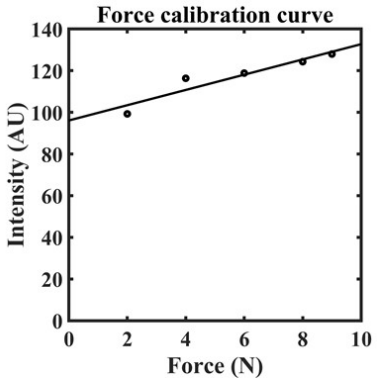


**FIGURE 12.** Calibration curve-based force versus the average number of red pixels.

### C. INTENSITY TO FORCE MEASUREMENT

The statistical differences between the low and high forces were measured based on the saturation channel from HSV, which represents the intensity colour level. The statistical comparison was presented using a histogram of intensity versus bin count, as shown in Fig. 11. The histogram demonstrates that the intensity variation is directly proportional to the force applied (intensity $\propto$ force applied). The bin count has a maximum peak at a certain intensity, represented by the magnitude of the force. In addition, the calibration curve of the force versus the number of pixels can be plotted, as shown in Fig. 12.

### D. IMPLEMENTATION OF A CALIBRATED FORCE MEASUREMENT TOOL TO CLEAR ALIGNER AND 3D TEETH MODEL

The intensity level determined from the histogram is directly proportional to the estimated force applied between the clear aligner and the teeth model. Therefore, a 3D topographical image was mapped with the saturation channel from the HSV colour space that implements the estimation of intensity and force. This process illustrates the level of force that was applied.

Next, the rectangular and ellipsoidal clear aligners were analysed using a similar image processing method with the force indicator. Figs. 13 (a) to (d) show the cropped and

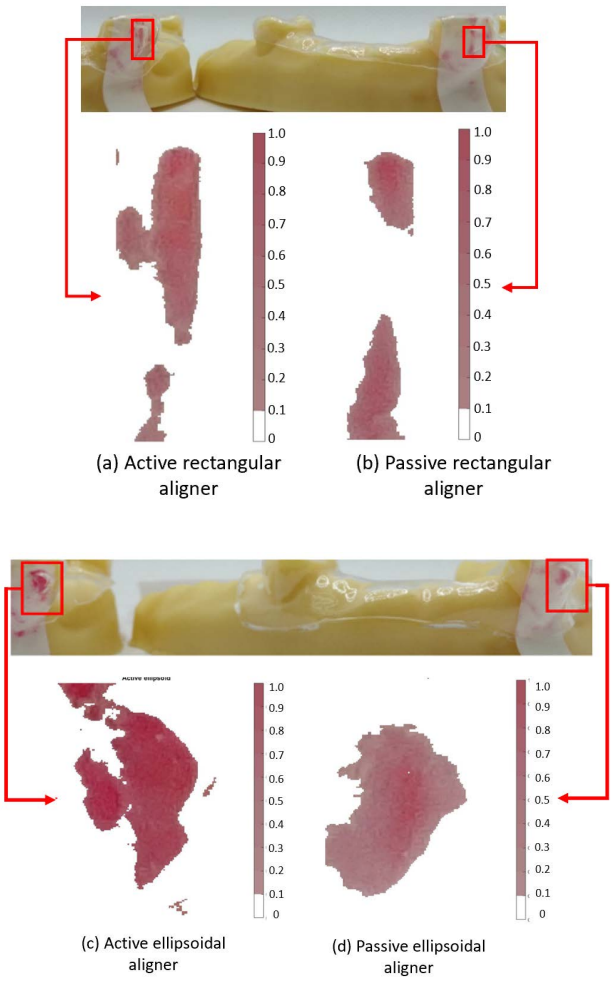


**FIGURE 13.** (a) Cropped and segmented image of rectangular active and passive attachment and (b) cropped and segmented image of ellipsoidal active and passive attachment.

segmented images of the rectangular and ellipsoidal attachments. The cropped image focuses on the sculpted part of the attachment, where the forces should differ between active and passive attachments. The application of the distributed force over specific areas of the tooth is then quantified using the image processing technique. This analysis allows the visualisation of the distributed force.

The 3D topographical map is obtained from the segmented image by plotting the forces in MATLAB. Figs. 14(a) to (d) show the two samples of rectangular attachments with active and passive aligners, respectively. The figures illustrate the force distribution exerted by the aligners onto the attachment surface. For the active rectangular attachment in Figs. 14(a) and (c), the force ranges from 5–10 N, localised around the middle of the sculpted area. In contrast, the forces in the passive rectangular attachment are significantly lower, as shown in Figs. 14 (b) and (d). The central region has a small force (less than 3 N). Around this region, the force is absent and therefore not mapped, which is expected as the passive aligner is not sculpted for any force exertion.

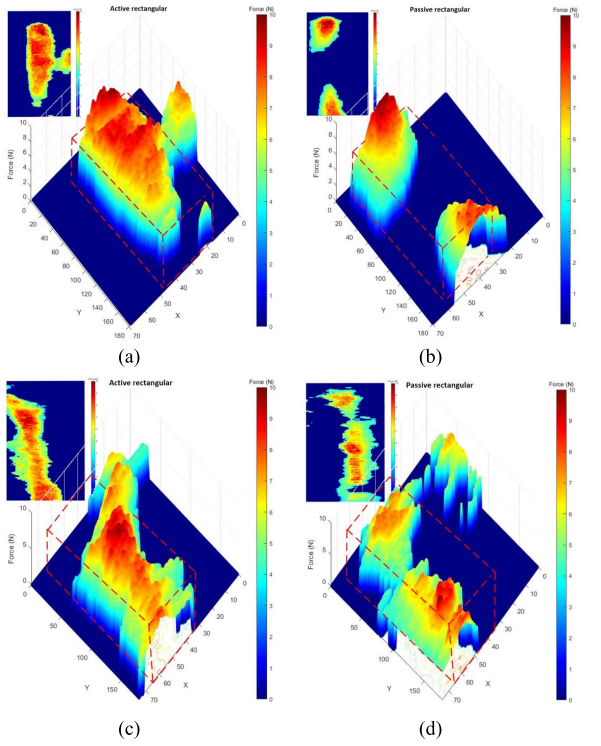


**FIGURE 14.** 3D maps of rectangular (a) active and (b) passive attachment (Sample 1); 3D maps of rectangular (c) active and (d) passive attachment (Sample 2).

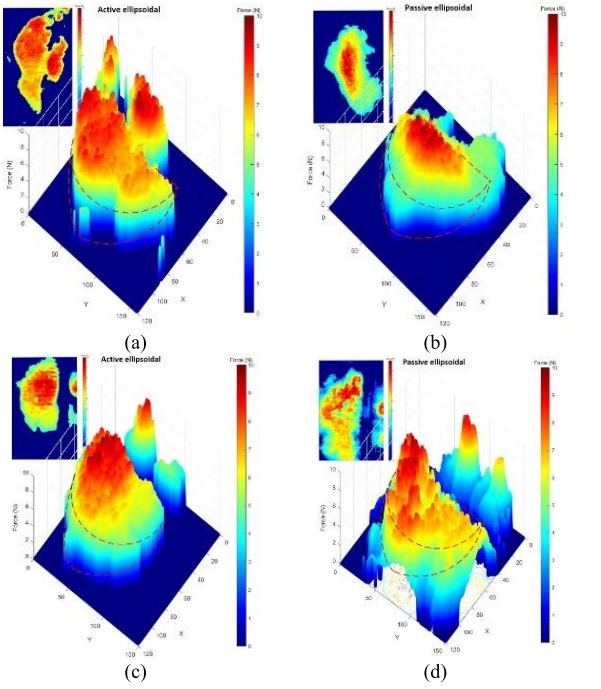


**FIGURE 15.** 3D maps of ellipsoidal (a) active and (b) passive attachment (Sample 1); 3D maps of ellipsoidal (c) active and (d) passive attachment (Sample 2).

Similarly, for the ellipsoidal attachment case in Figs. 15 (a) to (d), the active attachment shows the peak force at the sculpted area around the centre region. The same

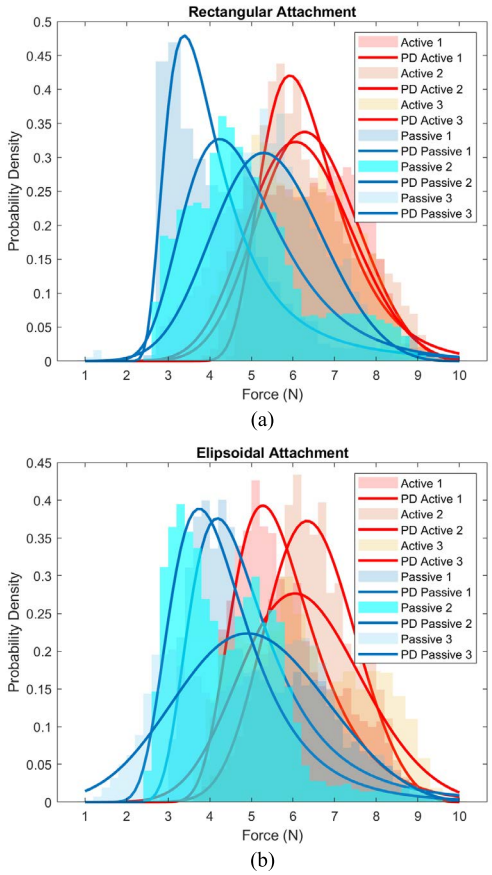


**FIGURE 16.** Sample of force distribution of (a) rectangular and (b) ellipsoidal attachment.

**TABLE 1.** A summary of the statistical parameter of force distribution.

| Shape | Type of aligner | No. of sample | Range of peak force (±1σ) | Standard deviation, σ | Mean, $\bar{x}$ |
|---|---|---|---|---|---|
| Ellipsoidal | Active | 1 | 5.224-7.514 | 1.145 | 6.369 |
| | | 2 | 5.308-7.567 | 1.129 | 6.438 |
| | | 3 | 5.005-7.417 | 1.206 | 6.211 |
| | Passive | 1 | 2.458-6.283 | 1.913 | 4.370 |
| | | 2 | 3.450-6.401 | 1.476 | 4.925 |
| | | 3 | 4.162-6.693 | 1.265 | 5.427 |
| Rectangular | Active | 1 | 4.615-7.033 | 1.209 | 5.824 |
| | | 2 | 5.394-7.470 | 1.038 | 6.432 |
| | | 3 | 4.858-7.701 | 1.422 | 6.279 |
| | Passive | 1 | 3.432-6.734 | 1.651 | 5.083 |
| | | 2 | 3.079-5.806 | 1.364 | 4.442 |
| | | 3 | 3.278-6.719 | 1.721 | 4.998 |

trend occurs for the passive aligner, but the intensity and distribution area is less, as expected. The force histogram is plotted in Fig. 15 to visualise the force composition.

Figs. 16(a) and (b) show the histogram plot and its corresponding best-fit probability density function curve. The best-fit curve was chosen using MATLAB based on the statistics toolbox. The most suitable probability density function was determined to be the GEV distribution. The statistical parameters, such as mean, variance and standard variation, were obtained from the MATLAB toolbox.

**TABLE 2.** Average mean of force different types of aligners.

| Shape | Aligner | Average of mean, $\bar{x}_{ave}$ | Average difference (Active−passive) |
|---|---|---|---|
| Ellipsoidal | Active | 6.179 | 1.338 |
| | Passive | 4.841 | |
| Rectangular | Active | 6.340 | 1.432 |
| | Passive | 4.908 | |

Table 1 summarises the statistical parameter of force distribution for all 12 samples. The range of the peak force was calculated by taking the difference in mean force value from one standard deviation. The equation is shown in (5).

$$\text{Range of peak force} = \bar{x} \pm \sigma \tag{5}$$

where $\bar{x}$ is the mean and $\sigma$ is the standard deviation. Three similar samples were analysed for each category to achieve consistency and repeatability of the force measurements on the aligners. For example, the peak force of the active aligner ranges from 4.6–7.7 N. In contrast, the peak force of the passive aligners ranges from 2.–6.7 N.

Table 2 summarises the mean for the different types of aligners, indicating that the mean for active aligners is consistently higher than that for the passive aligners. The average of mean value for each case is obtained by averaging the mean value in Table 1. This result shows that the active aligners produced higher localised forces on the attachments.

## IV. CONCLUSION

The level of force on the active attachment is higher than that on the passive attachment because the active attachment is supposed to direct force from the aligner to move the tooth in the desired direction. The results are consistent with this theory. The rectangular and ellipsoid buccal attachments delivered similar forces to the tooth. Both forces were lower than those delivered by a rectangular attachment on the palatal region of the tooth in other studies [58]. The attachment shape has little effect on bodily tooth movement [59]. Our results aligned, as the force distribution over rectangular and ellipsoid composite attachments were similar.

Our study demonstrated the mapping of the force distribution of the buccal rectangular and ellipsoid attachments, both active and passive. The composite attachment produces a moment to counteract the unfavourable inclination produced by aligners, which eventually produces a favourable tooth movement [48]. In our study, we measured the horizontal (seating pressure) and the vertical components of pressure [10]. The seating pressure is then eliminated by subtracting the value obtained from the passive aligner. Therefore, the average net force from the attachment exerted was 1.3–1.4 N. This result is comparable to values measured by Cervinara *et al.* [12], another in-vitro study using resin models and pressure films, but without the additional images of topographical mapping obtained in our study.

One of our study's limitations was that the experiment was conducted in-vitro, where the presence of alveolar bones and

the periodontal ligament was not simulated. Their presence might alter the net force delivered to the teeth, owing to the viscoelastic properties of the periodontal ligament that distribute force into the bone. In in-vitro studies, the main challenge is simulating the force in humans [51]. In fixed-appliance treatment for rotation movements, the theory of net force by Proffit is roughly 0.5 N [60]. In this lab study, since a resin model was used, the teeth did not move with the attachment without the periodontal ligament. Therefore, the range of forces was expected to be considerably higher (1.3–1.4 N). This observation is similar to other resin model studies, which recorded higher and similar-ranged forces [12]. The study also focuses on the force exerted on a single attachment rather than on the whole tooth or whole arch. Therefore, the results should be interpreted for the attachment only. A future extensive study that is in-vivo in nature is warranted. However, this preliminary finding can lead to the effective exploration of topographical mapping in the clinical setting.

The proposed topographical pressure mapping system clearly visualised the distributed force on the clear aligner attachment. For active attachments, the mean force ranges from 6.2–6.3 N. In contrast, for the passive aligners, the mean force ranges from 4.8–4.9 N. Therefore, the average net force from the attachment exerted was 1.3–1.4 N. The preliminary results obtained in our study showed how the actual topographical mapping of forces could be obtained. Despite the implementation of image colour space conversion has been done more than once, the integrity and reliability of the image are preserved and not affected. This method will be a valuable tool in the clinical, research, and commercial field. In terms of clinical, mor comprehensive studies could compare the findings to the theory of orthodontic tooth movement. This technique can also be a reference method to identify the optimum force for tooth movement in treatment using aligners. It also allows practitioners and patients to understand better how the attachments on aligners work and why they need to be in a specific location on the teeth. A patient would appreciate visual data rather than just descriptive data. In terms of research, there have been many types of research focusing on orthodontic appliances and how they are associated with pain, where in general clear aligners are found to be less painful in terms of patient-reported outcomes. Having the actual forces measured would quantify data on their association with pain. Commercially, this unique method could be used in many other aligner companies to allow for evaluation and quality purposes. Furthermore, the preliminary finding of this work could be developed further to be used as a reference in future clinical orthodontic clear aligner and attachment research.

## ACKNOWLEDGMENT

The authors would like to express their gratitude to the technicians, especially Daniel Liam from WhiteSmileclear Laboratory Services, for their assistance and supporting staff from Universiti Kebangsaan Malaysia (UKM).

## REFERENCES

[1] A. Ashari and A. M. Mohamed, "Relationship of the dental aesthetic index to the oral health-related quality of life," *Angle Orthodontist*, vol. 86, no. 2, pp. 337–342, Mar. 2016, doi: 10.2319/121014-896.1.

[2] M. Gao, X. Yan, R. Zhao, Y. Shan, Y. Chen, F. Jian, H. Long, and W. Lai, "Comparison of pain perception, anxiety, and impacts on oral health-related quality of life between patients receiving clear aligners and fixed appliances during the initial stage of orthodontic treatment," *Eur. J. Orthodontics*, vol. 43, no. 3, pp. 353–359, 2020, doi: 10.1093/ejo/cjaa037.

[3] T. Weir, "Clear aligners in orthodontic treatment," *Austral. Dental J.*, vol. 62, pp. 58–62, Mar. 2017, doi: 10.1111/adj.12480.

[4] Q. Jiang, J. Li, L. Mei, J. Du, L. Levrini, G. M. Abbate, and H. Li, "Periodontal health during orthodontic treatment with clear aligners and fixed appliances: A meta-analysis," *J. Amer. Dental Assoc.*, vol. 149, no. 8, pp. 712–720, 2018, doi: 10.1016/j.adaj.2018.04.010.

[5] A. Iliadi, D. Koletsi, and T. Eliades, "Forces and moments generated by aligner-type appliances for orthodontic tooth movement: A systematic review and meta-analysis," *Orthodontics Craniofacial Res.*, vol. 22, no. 4, pp. 248–258, Nov. 2019, doi: 10.1111/ocr.12333.

[6] F. Yazid, Y. Teh, A. Ashari, S. H. Z. Ariffin, and R. M. A. Wahab, "Detection methods of orthodontically induced inflammatory root resorption (OIIRR): A review," *Australas. Orthodontic J.*, vol. 36, no. 1, pp. 101–107, Jan. 2020.

[7] G. Rossini, S. Parrini, T. Castroflorio, A. Deregibus, and C. L. Debernardi, "Efficacy of clear aligners in controlling orthodontic tooth movement: A systematic review," *Angle Orthodontist*, vol. 85, no. 5, pp. 881–889, Sep. 2015, doi: 10.2319/061614-436.1.

[8] R. M. A. Wahab, Z. Yamamoto, A. Sintian, N. A. Kasim, I. Z. Z. Abidin, S. Senafi, Z. Z. Ariffin, and S. H. Z. Ariffin, "The effects of orthodontic forces during canine retraction using self-ligating brackets on gingival crevicular fluid enzyme activity, canine movement and root resorption," *Sains Malaysiana*, vol. 44, no. 2, pp. 249–256, Feb. 2015, doi: 10.17576/jsm-2015-4402-12.

[9] Y. Kitafusa, "Application of 'prescale' as an aid to clinical diagnosis in orthodontics," *Bull. Tokyo Dental College*, vol. 45, no. 2, pp. 99–108, 2004, doi: 10.2209/tdcpublication.45.99.

[10] T. P. Verma, K. I. Kumathalli, V. Jain, and R. Kumar, "Bite force recording devices—A review," *J. Clin. Diagnostic Res.*, vol. 11, no. 9, pp. 1–5, 2017, doi: 10.7860/JCDR/2017/27379.10450.

[11] M. Takahashi, F. Takahashi, and O. Morita, "Evaluation of the masticatory part and the habitual chewing side by wax cube and bite force measuring system (dental prescale)," *Nihon Hotetsu Shika Gakkai Zasshi*, vol. 52, no. 4, pp. 513–520, 2008, doi: 10.2186/jjps.52.513.

[12] F. Cervinara, C. Cianci, F. D. Cillis, G. Pappalettera, C. Pappalettere, G. Siciliani, and L. Lombardo, "Experimental study of the pressures and points of application of the forces exerted between aligner and tooth," *Nanomaterials*, vol. 9, no. 7, pp. 1–9, 2019, doi: 10.3390/nano9071010.

[13] M. Jalalpour, J. J. Kim, and M. M. R. Taha, "Monitoring of L-shape bolted joint tightness using thermal contact resistance," *Exp. Mech.*, vol. 53, no. 9, pp. 1531–1543, Nov. 2013, doi: 10.1007/s11340-013-9759-9.

[14] L. J. Barbagallo, G. Shen, A. S. Jones, M. V. Swain, P. Petocz, and M. A. Darendeliler, "A novel pressure film approach for determining the force imparted by clear removable thermoplastic appliances," *Ann. Biomed. Eng.*, vol. 36, no. 2, pp. 335–341, Feb. 2008, doi: 10.1007/s10439-007-9424-5.

[15] R. C. Hrosik, E. Tuba, E. Dolicanin, R. Jovanovic, and M. Tuba, "Brain image segmentation based on firefly algorithm combined with *K*-means clustering," *Stud. Informat. Control*, vol. 28, no. 2, pp. 167–176, Jul. 2019, doi: 10.24846/v28i2y201905.

[16] I. E. Kaya, A. Ç. Pehlivanı, E. G. Sekizkardeş, and T. Ibrikci, "PCA based clustering for brain tumor segmentation of T1w MRI images," *Comput. Methods Programs Biomed.*, vol. 140, pp. 19–28, Mar. 2017, doi: 10.1016/j.cmpb.2016.11.011.

[17] I. Cabria and I. Gondra, "MRI segmentation fusion for brain tumor detection," *Inf. Fusion*, vol. 36, pp. 1–9, Jul. 2017, doi: 10.1016/j.inffus.2016.10.003.

[18] J. Su, S. Liu, and J. Song, "A segmentation method based on HMRF for the aided diagnosis of acute myeloid leukemia," *Comput. Methods Programs Biomed.*, vol. 152, pp. 115–123, Dec. 2017, doi: 10.1016/j.cmpb.2017.09.011.

[19] H. D. Cheng, X. H. Jiang, Y. Sun, and J. Wang, "Color image segmentation: Advances and prospects," *Pattern Recognit.*, vol. 34, no. 12, pp. 2259–2281, Dec. 2001, doi: 10.1016/S0031-3203(00)00149-7.

[20] D. J. Bora, "Importance of image enhancement techniques in color image segmentation: A comprehensive and comparative study," *Indian J. Sci. Res.*, vol. 15, no. 1, pp. 115–131, 2017.
[21] H. S. Pransantha, "Image segmentation algorithms on digital signal processor," *Int. J. Creative Res. Thoughts*, vol. 8, no. 8, pp. 2320–2882, 2020.
[22] S. Barui, S. Latha, D. Samiappan, and P. Muthu, "SVM pixel classification on colour image segmentation," *J. Phys., Conf. Ser.*, vol. 1000, no. 1, pp. 1–4, 2018, doi: 10.1088/1742-6596/1000/1/012110.
[23] MathWorks. (2020). *Convert RGB to CIE 1976 L*a*b*—MATLAB rgb2lab*. Accessed: Nov. 3, 2020. [Online]. Available: https://www.mathworks.com/help/images/ref/rgb2lab.html?s_tid=srchtitle
[24] Z. Wang, "Robust segmentation of the colour image by fusing the SDD clustering results from different colour spaces," *IET Image Process.*, vol. 14, no. 13, pp. 3273–3281, Nov. 2020, doi: 10.1049/iet-ipr.2019.1481.
[25] A. Hanbury and J. Serra, "Mathematical morphology in the L*a*b* colour space," Centre de Morphologie Mathématique, Fontainebleau Cedex, France, Tech. Rep. N-36/01/MM-30, Aug. 2001.
[26] S. R. Abdani, W. M. D. W. Zaki, A. Mustapha, and A. Hussain, "Iris segmentation method of pterygium anterior segment photographed image," in *Proc. IEEE Symp. Comput. Appl. Ind. Electron. (ISCAIE)*, Apr. 2015, pp. 69–72, doi: 10.1109/ISCAIE.2015.7298330.
[27] R. M. Haralick and L. G. Shapiro, "Image segmentation techniques," *Comput. Vis., Graph., Image Process.*, vol. 29, no. 1, pp. 100–132, 1985, doi: 10.1016/S0734-189X(85)90153-7.
[28] A. Coates and A. Y. Ng, "Learning feature representations with *K*-means," in *Neural Networks: Tricks of the Trade*. Berlin, Germany: Springer, 2012, pp. 561–580, doi: 10.1007/978-3-642-35289-8_30.
[29] A. Lawrynowicz and V. Tresp, "Introducing machine learning," *Perspect. Ontol. Learn.*, vol. 2, no. 1, pp. 35–48, 2011, doi: 10.1111/j.2041-210X.2010.00056.x.
[30] Z. Jiang, Y. Zheng, H. Tan, B. Tang, and H. Zhou, "Variational deep embedding: An unsupervised and generative approach to clustering," in *Proc. 26th Int. Joint Conf. Artif. Intell.*, Aug. 2017, pp. 1–22, doi: 10.24963/ijcai.2017/273.
[31] N. S. M. Zamani, W. M. D. W. Zaki, A. B. Huddin, A. Hussain, H. A. Mutalib, and A. Ali, "Automated pterygium detection using deep neural network," *IEEE Access*, vol. 8, pp. 191659–191672, 2020, doi: 10.1109/access.2020.3030787.
[32] S. N. A. Ahmad, W. M. D. W. Zaki, and N. S. M. Zamani, "A pterygium disease screening system for anterior segment photographed images," *J. Kejuruteraan*, vol. 31, no. 1, pp. 99–105, 2019.
[33] M. Caron, P. Bojanowski, A. Joulin, and M. Douze, "Deep clustering for unsupervised learning of visual features," in *Proc. Eur. Conf. Comput. Vis.*, 2018, pp. 132–149, doi: 10.1007/978-3-030-01264-9_9.
[34] J. Xu and K. Lange, "Power *k*-means clustering," in *Proc. 36th Int. Conf. Mach. Learn. (ICML)*, vol. 97, 2019, pp. 6921–6931.
[35] J. MacQueen, "Some methods for classification and analysis of multivariate observations," in *Proc. 5th Berkeley Symp. Math. Stat. Probab.*, 1967, vol. 1, no. 14, pp. 281–297.
[36] C. Yuan and H. Yang, "Research on *k*-value selection method of *k*-means clustering algorithm," *J-Multidisciplinary Sci. J.*, vol. 2, no. 2, pp. 226–235, 2019, doi: 10.3390/j2020016.
[37] L. Liu, B. He, J. Zhuang, L. Zhang, and A. Lv, "Force measurement system for invisalign based on thin film single force sensor," *Measurement*, vol. 97, pp. 1–7, Feb. 2017, doi: 10.1016/j.measurement.2016.11.018.
[38] A. B. Liggins, J. C. E. Stranart, J. B. Finlay, and C. H. Rorabeck, "Calibration and manipulation of data from Fuji pressure-sensitive film," in *Experimental Mechanics: Technology Transfer Between High Tech Engineering and Biomechanics*, 1st ed. Amsterdam, The Netherlands: Elsevier, 1992, pp. 61–70.
[39] F. Becker, R. Jäger, F. Schmidt, B. Lapatki, and O. Paul, "Miniaturized six-degree-of-freedom force/moment transducers for instrumented teeth," *IEEE Sensors J.*, vol. 17, no. 12, pp. 3644–3655, Jun. 2017, doi: 10.1109/JSEN.2017.2696035.
[40] M. Juneja, P. Jindal, D. Bajaj, I. Madhav, and R. Tuli, "Methodology for stress measurement by transparent dental aligners using strain gauge," *World J. Dentistry*, vol. 9, no. 1, pp. 13–18, Feb. 2018, doi: 10.5005/jp-journals-10015-1499.
[41] M. Mencattelli, E. Donati, M. Cultrone, and C. Stefanini, "Novel universal system for 3-dimensional orthodontic force-moment measurements and its clinical use," *Amer. J. Orthodontics Dentofacial Orthopedics*, vol. 148, no. 1, pp. 174–183, Jul. 2015, doi: 10.1016/j.ajodo.2015.01.028.
[42] F. Elkholy, F. Schmidt, R. Jäger, and B. G. Lapatki, "Forces and moments applied during derotation of a maxillary central incisor with thinner aligners: An *in-vitro* study," *Amer. J. Orthodontics Dentofacial Orthopedics*, vol. 151, no. 2, pp. 407–415, Feb. 2017, doi: 10.1016/j.ajodo.2016.08.020.
[43] H. A. Colosi, M. N. Roman, and A. A. Cadariu, "Numerical simulation of periodontal stress distribution during orthodontic tipping of single rooted teeth," in *Proc. IEEE Int. Conf. Autom., Quality Test., Robot.*, May 2006, pp. 430–432, doi: 10.1109/AQTR.2006.254674.
[44] K. Shimoda, H. Takemura, Y. Obara, M. Shigeta, K. Soga, K. Suga, W.-J. Lai, S. Kim, Z. Kanno, and M. Uo, "Development of 6-axis orthodontic force and moment sensing device for decreasing accident of orthodontic treatment," in *Proc. 40th Annu. Int. Conf. IEEE Eng. Med. Biol. Soc. (EMBC)*, Jul. 2018, pp. 1797–1800, doi: 10.1109/EMBC.2018.8512648.
[45] A. Cortona, G. Rossini, S. Parrini, A. Deregibus, and T. Castroflorio, "Clear aligner orthodontic therapy of rotated mandibular round-shaped teeth: A finite element study," *Angle Orthodontist*, vol. 90, no. 2, pp. 247–254, Mar. 2020, doi: 10.2319/020719-86.1.
[46] J. Wu, Y. Liu, J. Zhang, W. Peng, and X. Jiang, "Biomechanical investigation of orthodontic treatment planning based on orthodontic force measurement and finite element method before implementation: A case study," *Technol. Health Care*, vol. 26, pp. 347–359, May 2018, doi: 10.3233/THC-174689.
[47] B. Comba, S. Parrini, G. Rossini, T. Castroflorio, and A. Deregibus, "A three-dimensional finite element analysis of upper-canine distalization with clear aligners, composite attachments, and class II elastics," *J. Clin. Orthodontics*, vol. 51, pp. 24–28, Jan. 2017.
[48] J. P. Gomez, F. M. Peña, V. Martínez, D. C. Giraldo, and C. I. Cardona, "Initial force systems during bodily tooth movement with plastic aligners and composite attachments: A three-dimensional finite element analysis," *Angle Orthodontist*, vol. 85, no. 3, pp. 454–460, May 2015, doi: 10.2319/050714-330.1.
[49] W. Hahn, H. Dathe, J. Fialka-Fricke, S. Fricke-Zech, A. Zapf, D. Kubein-Meesenburg, and R. Sadat-Khonsari, "Influence of thermoplastic appliance thickness on the magnitude of force delivered to a maxillary central incisor during tipping," *Amer. J. Orthodontics Dentofacial Orthopedics*, vol. 136, no. 1, pp. 121–127, 2009, doi: 10.1016/j.ajodo.2008.12.015.
[50] W. Hahn, B. Engelke, K. Jung, H. Dathe, J. Fialka-Fricke, D. Kubein-Meesenburg, and R. Sadat-Khonsari, "Initial forces and moments delivered by removable thermoplastic appliances during rotation of an upper central incisor," *Angle Orthodontist*, vol. 80, no. 2, pp. 239–246, Mar. 2010, doi: 10.2319/033009-181.1.
[51] W. Hahn, A. Zapf, H. Dathe, J. Fialka-Fricke, S. Fricke-Zech, R. Gruber, D. Kubein-Meesenburg, and R. Sadat-Khonsari, "Torquing an upper central incisor with aligners-acting forces and biomechanical principles," *Eur. J. Orthodontics*, vol. 32, no. 6, pp. 607–613, Dec. 2010, doi: 10.1093/ejo/cjq007.
[52] A. Skaik, X. L. Wei, I. Abusamak, and I. Iddi, "Effects of time and clear aligner removal frequency on the force delivered by different polyethylene terephthalate glycol-modified materials determined with thin-film pressure sensors," *Amer. J. Orthodontics Dentofacial Orthopedics*, vol. 155, no. 1, pp. 98–107, Jan. 2019, doi: 10.1016/j.ajodo.2018.03.017.
[53] N. Kohda, M. Iijima, T. Muguruma, W. A. Brantley, K. S. Ahluwalia, and I. Mizoguchi, "Effects of mechanical properties of thermoplastic materials on the initial force of thermoplastic appliances," *Angle Orthodontist*, vol. 83, no. 3, pp. 476–483, May 2013, doi: 10.2319/052512-432.1.
[54] *Pressure Measurement Film Prescale*, Fujifilm Holdings Corp., Tokyo, Japan, 2012.
[55] A. B. Liggins, W. R. Hardie, and J. B. Finlay, "The spatial and pressure resolution of Fuji pressure-sensitive film," *Exp. Mech.*, vol. 35, no. 2, pp. 166–173, Jun. 1995, doi: 10.1007/BF02326476.
[56] N. Otsu, "A threshold selection method from gray-level histograms," *IEEE Trans. Syst., Man, Cybern.*, vol. SMC-9, no. 1, pp. 62–66, Jan. 1979.
[57] P. Ganesan, V. Rajini, B. S. Sathish, and K. B. Shaik, "HSV color space based segmentation of region of interest in satellite images," in *Proc. Int. Conf. Control, Instrum., Commun. Comput. Technol. (ICCICCT)*, Jul. 2014, pp. 101–105, doi: 10.1109/ICCICCT.2014.6992938.
[58] R. Savignano, R. Valentino, A. V. Razionale, A. Michelotti, S. Barone, and V. D'Antò, "Biomechanical effects of different auxiliary-aligner designs for the extrusion of an upper central incisor: A finite element analysis," *J. Healthcare Eng.*, vol. 2019, pp. 1–9, Aug. 2019, doi: 10.1155/2019/9687127.
[59] C.-T. Ho, Y.-T. Huang, C.-W. Chao, T.-H. Huang, and C.-T. Kao, "Effects of different aligner materials and attachments on orthodontic behavior," *J. Dental Sci.*, vol. 16, no. 3, pp. 1001–1009, Jul. 2021, doi: 10.1016/j.jds.2021.01.011.

[60] W. R. Proffit and H. W. Fields, *Contemporary Orthodontics*, 3rd ed. St. Louis, MO, USA: Mosby, 2000.

**N. SYAHIRA M. ZAMANI** received the B.Eng. degree in computer and communication engineering from Universiti Kebangsaan Malaysia (UKM), Bangi, Malaysia, in 2017, where she is currently pursuing the M.S. degree in system engineering. She is also working as a Graduate Research Assistant with the Department of Electrical, Electronic and Systems Engineering, Faculty of Engineering and Built Environment, UKM. Her research interests include image processing and artificial intelligence systems.

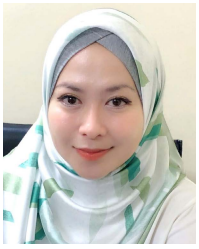

**ASMA ASHARI** received the bachelor's degree in dental surgery from the University of Adelaide, Australia. She is currently a Specialist and a Dental Lecturer with the Department of Family Oral Health, Faculty of Dentistry, Universiti Kebangsaan Malaysia. Her research interests include clinical orthodontics, aesthetic orthodontic appliances, orthodontic retention, oral health quality of life in orthodontics, and root resorption in orthodontics. She underwent specialist training with the Queen Mary University of London. She has passed her membership in orthodontics with the Royal College of Surgeons Edinburgh. She was awarded the Robert Lee Award by Royal London Hospital Alumni and the Dental Clinical and Education Experience Fellowship by the Royal College of Surgeons of Edinburgh.

**SAWAL HAMID MD ALI** (Member, IEEE) received the M.Sc. and Ph.D. degrees from the University of Southampton, U.K., in 2004 and 2010, respectively. He is currently a Professor in embedded systems with the Department of Electrical, Electronic and Systems Engineering, Faculty of Engineering and Built Environment, Universiti Kebangsaan Malaysia (UKM). His current research interests include wearable systems, system-on-chip design, and pervasive computing.

**KOK BENG GAN** (Member, IEEE) was born in Malaysia, in June 1978. He received the B.S. degree in material physics from University Technology Malaysia, in 2001, and the Ph.D. degree in electrical, electronic, and system engineering from Universiti Kebangsaan Malaysia, in 2009. He was an Engineer in the field of electronic manufacturing services and original design manufacturing, from 2001 to 2005. After several years of industry experience, he decided to venture into academic, in 2005. He is currently an Associate Professor with the Department of Electrical, Electronic and Systems Engineering, Faculty of Engineering and Built Environment, Universiti Kebangsaan Malaysia. He specializes in embedded systems in healthcare. His current research interests include biomedical optics, optical instrumentation, embedded systems, signal processing for medical application and biomechanics, and human motion analysis.

**REUBEN AXEL WEE MING HOW** received the degree from the University of Otago, in 2000. He won the Ivoclar Prize for undergraduate research, in 2000. He undertook specialist training in clinical orthodontics with the University of Edinburgh and completing the membership examination in orthodontic with the Royal College of Surgeons, in 2007. He was also awarded the membership in orthodontics of the Royal Australasian College of Dental Surgeons, in 2007. Apart from holding prior academic appointments at University Kebangsaan Malaysia, he is currently practicing orthodontics in private practice with the WhiteSmileclear Laboratory Services, Kuala Lumpur, Malaysia. His research interest includes bridging the biological delivery of clear aligner treatment.

**ROHAYA MEGAT ABDUL WAHAB** received the bachelor's degree in dental surgery from the University of Malaya, Malaysia, in 1994. She underwent specialist orthodontic training with the Leeds Dental Institute, Leeds, U.K., and a membership in orthodontics with the Royal College of Surgeons of Edinburgh, in 2001. She is currently a Professor in orthodontics with the Department of Family Oral Health, Faculty of Dentistry, Universiti Kebangsaan Malaysia. Her research interests include biomarkers in tooth movement and root resorption, stem cell therapy in bone regenerative for cleft lip, and palate patients.

**ALIZAE MARNY FADZLIN SYED MOHAMED** received the bachelor's degree in dental surgery from the University of Malaya, in 1997. She undertook specialist orthodontic training with the Kings College London, Guys Dental Institute, followed by a membership in orthodontics with the Royal College of Surgeons of Edinburgh, in 2005, and her consultant appointments were verified, in 2005. Currently, she is an Associate Professor with the Department of Family Oral Health, Faculty of Dentistry, Universiti Kebangsaan Malaysia. Her research interests include dental education and 3D models and its applications.

**SINDHU SINNASAMY** received the bachelor's degree in dental surgery from the University of Malaya, in 2010. She is currently undergoing specialty training of Doctorate degree in orthodontics with the Faculty of Dentistry, Mahsa University, and International Islamic University of Malaysia. Her research interests include the field of orthodontics and treatment outcomes.

**MOHD HADRI HAFIZ MOKHTAR** (Member, IEEE) received the M.Eng. degree in electrical and electronics from the University of Birmingham, U.K., in 2009, and the Ph.D. degree in electrical engineering from the Imperial College London, in 2016. He is currently a Senior Lecturer with the Department of Electrical, Electronic and Systems Engineering, Faculty of Engineering and Built Environment, Universiti Kebangsaan Malaysia. His research interests include fibre-based optical imaging, optical scanning microscopy, and optical sensors.